NON-EXTENSIVE THERMODYNAMICS, HEAVY ION COLLISIONS AND PARTICLE PRODUCTION AT RHIC ENERGIES

BHASKAR DE

Department of Physics, Moulana Azad College,
8, Rafi Ahmed Kidwai Road, Kolkata 700013, India
de_bhaskar@yahoo.com

S. BHATTACHARYYA*

Physics and Applied Mathematics Unit (PAMU),
Indian Statistical Institute, Kolkata 700108, India
bsubrata@www.isical.ac.in

GOUTAM SAU

Beramara Ramchandrapur High School,
South 24-Pgs, 743609(WB), India
gautamsau@yahoo.co.in

S. K. BISWAS

West Kodalia Adarsha Siksha Sadan, New Barrackpore,
Kolkata-700131, India
suniLbiswas2004@yahoo.com

Received 16 August 2006

In the light of ideas of the nonextensive thermodynamics, we have analyzed here the transverse momentum spectra of pions and protons produced at different centralities in the interactions of $P + P$, $D + Au$ and $Au + Au$ interactions, all of them at $\sqrt{s_{NN}} =$ 200 GeV at RHIC-BNL. Comparison of the results and the comments thereon have also been made with indications of suitable hints to the physical import and implications. The overall impact and the utility of the approach along with the obtained results are discussed in detail.

Keywords: Relativistic heavy ion collision; inclusive cross section.

PACS Number(s): 25.75.-q, 13.60.Hb

*Corresponding author.

1. Introduction

Since Tsallis introduced his nonextensive statistical mechanics,[1] the theory has found wide applicability in various branches of physics. Tsallis' formalism for nonextensive entropy was a generalization of Boltzmann Statistics. There are various physical phenomena which can be described with a considerable degree of precision by this nonextensive statistics. The field of Heavy Ion Physics is also no exception. The transverse momentum spectra of different secondaries obtained from a high energy nuclear interaction exhibit power-law-like behavior, specially at high transverse momenta region. This deviation from a purely exponential-like behavior of the transverse momentum spectra can throw light on the thermodynamical properties of hot and dense nuclear matter formed in nuclear collisions at relativistic energies if a suitable formalism, like nonextensive thermodynamics, is adopted in analyzing the experimental data. In fact, some efforts have already been made in this regard[2–9] in the recent past, though a comprehensive work is yet to be done. We have taken up, here in the present work, the task of analyzing the transverse momentum spectra of positively charged pi-mesons and protons–antiprotons produced in different centralities in $Au+Au$ collisions alongwith $D+Au$ and $P+P$ collisions. However, the study here pertains only to the RHIC-data at $\sqrt{s_{NN}} = 200$ GeV, so that a comparison between different collisions could be made on an equal footing. But even for RHIC energy at $\sqrt{s_{NN}} = 130$ GeV the available data is relatively sparse to test validity of the approach.

Among the particles produced, pions constitute the most dominant variety in the three possible charge states. Of them, the data on neutral pions have been dealt with by Biyajima *et al.*,[8,9] but the production of the charged variety has still not been taken up. We now focus on them, especially on pions and protons.

Noticeably, in the present study, we have left out the production of kaons because of the fact that the p_T-ranges of the data on kaons — even in the marginal high-p_T domain — are quite narrow in all the reports on the experimental measurements. So, it is difficult to arrive at any decisive conclusion on their behavior with relatively sparse data and narrow p_T-range.

The outline of this paper is as follows: In the next section (Sec. 2) we give a brief introduction to the nonextensive statistics and the main working formula to be used in our work here. The results are reported in Sec. 3 with some specific observations made. And in the last section we present our conclusions.

2. Nonextensive Statistics and Transverse Momentum Spectra

The nonextensive entropy by Tsallis generalized statistics[1] is given by

$$S_q = \frac{1}{q-1}\left(1 - \sum_i p_i^q\right) \tag{1}$$

where p_i are probabilities associated with the microstates of a physical system and q is the nonextensivity parameter. For $q \to 1$, Eq. (1) gives the ordinary Boltzmann–

Gibbs entropy

$$S = -\sum_i p_i \ln p_i \,. \tag{2}$$

The generalized statistics of Tsallis is not only applicable to an equilibrium system, but also to nonequilibrium systems with stationary states.[3] As the name "nonextensive" implies, these entropies are not additive for independent systems. For a system of N independent particles, the Hamiltonian in nonextensive approach[3] is given by

$$H = \sum_j \epsilon_{i_j} + (q-1)\beta \sum_{j,k} \epsilon_{i_j}\epsilon_{i_k} + (q-1)^2\beta^2 \sum_{j,k,l} \epsilon_{i_j}\epsilon_{i_k}\epsilon_{i_l} + \cdots \tag{3}$$

where ϵ_{i_j} is the energy of particle j in ith energy state, and $\beta = 1/T$ is the inverse temperature variable. The above equation clearly indicates that for a non-extensive system the total energy is not the sum of the single-particle energies.

The energy associated with a particle denoted by j in a momentum state i in a fireball produced in a high energy nuclear collision is given by

$$\epsilon_{ij} = \sqrt{\mathbf{p}_i^2 + m_j^2}\,. \tag{4}$$

The non-extensive Boltzmann factor[3] is defined as

$$x_{ij} = (1 + (q-1)\beta\epsilon_{ij})^{-q/(q-1)} \tag{5}$$

with $q \to 1$, the above equation approaches the ordinary Boltzmann factor $e^{-\beta\epsilon_{ij}}$. If ν_{ij} denotes the number of particles of type j in momentum state i, the generalized grand canonical partition function is given by

$$Z = \sum_{(\nu)} \prod_{ij} x_{ij}^{\nu_{ij}} \,. \tag{6}$$

The average occupation number of a particle of species j in the momentum state i can be written as[3]

$$\bar{\nu}_{ij} = x_{ij} \frac{\partial}{\partial x_{ij}} \log Z = \frac{1}{(1 + (q-1)\beta\epsilon_{ij})^{q/(q-1)} \pm 1} \tag{7}$$

where the $-$ sign is for bosons and the $+$ sign is for fermions. Using the above relationships, the probability density $w(p_T)$ of a particle of rest mass m_0 and of transverse momentum p_T is given by

$$w(p_T) = const.\;\; p_T \int_0^\infty dp_L \frac{1}{(1 + (q-1)\beta\sqrt{p_T^2 + p_L^2 + m_0^2})^{q/(q-1)} \pm 1} \,. \tag{8}$$

Since the temperature T, which will be termed here as Hagedorn temperature and is denoted as T_0, is quite small, i.e., $\beta\sqrt{p_T^2 + p_L^2 + m_0^2} \gg 1$, one can neglect ± 1 in the denominator of the previous equation. Hence, the differential cross section, which is proportional to $w(p_T)$, can be expressed as

$$\frac{1}{\sigma}\frac{d\sigma}{dp_T} \approx c p_T \int_0^\infty dp_L (1 + (q-1)\beta\sqrt{p_T^2 + p_L^2 + m_0^2})^{-q/(q-1)} \tag{9}$$

where c is a constant of proportionality. Equation (9) provides the working formula for present analysis.

3. Results

The diagrams in Figs. 1 to 4 present the main body of our main results. They present the degree of agreement between measured data and the results attainable by the approach based on non-extensive thermodynamics. The diagrams Figs. 1(a)

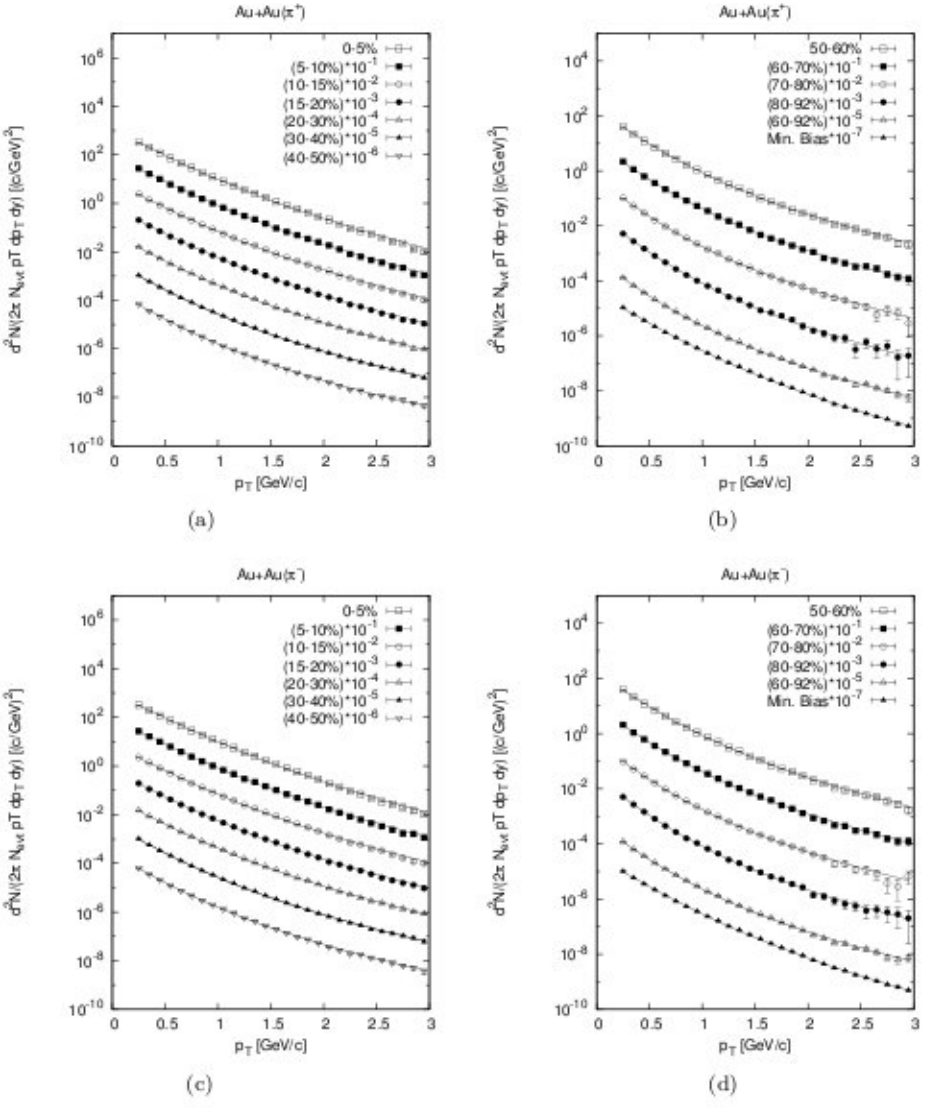

Fig. 1. Plots of transverse momentum spectra of $\pi^{\pm}$ produced in $Au + Au$ collisions at $\sqrt{s} =$ 200 GeV at different centralities. The filled symbols represent the experimental data points.[10–12] The solid curves provide the fits on the basis of nonextensive approach (Eq. (9)).

to 1(d) are drawn theoretically for the production of pions in $Au + Au$ collision at $\sqrt{s_{NN}} = 200$ GeV and they are for various centralities. The plots in Fig. 2 are for production of protons–antiprotons in the same collision and at the same energy, but for varying centrality. The figures in Fig. (3) depict the results for $D + Au$ collision at the same energy but for varying centralities. Those in Fig. 4 present the fits to data in $P + P$ collision. Besides, the plots in Figs. 5 to 8 show up the properties of the non-extensivity parameter (q) and of the temperature

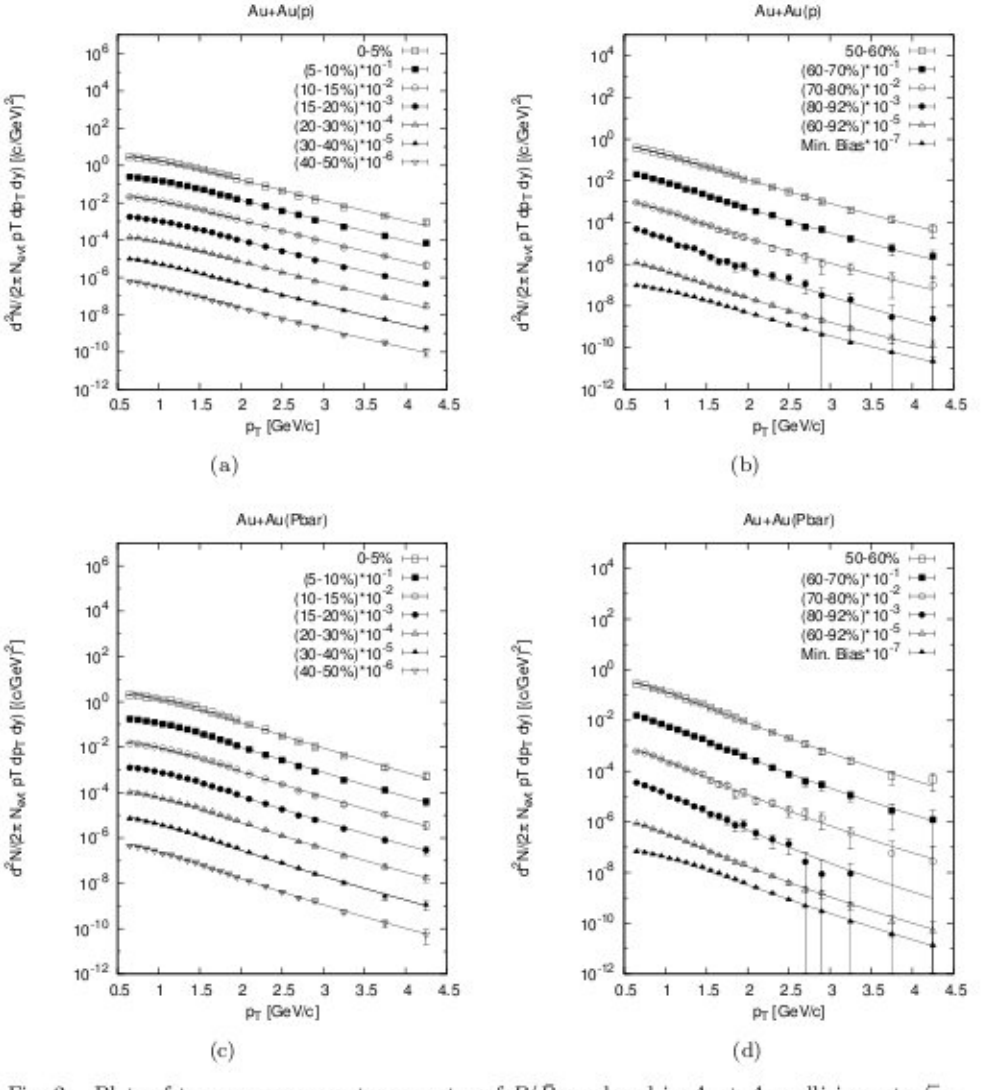

Fig. 2. Plots of transverse momentum spectra of $P/\bar{P}$ produced in $Au + Au$ collisions at $\sqrt{s} =$ 200 GeV at different centralities. The filled symbols represent the experimental data points.[10–12] The solid curves provide the fits on the basis of nonextensive approach (Eq. (9)).

(T_0) in terms of the number of participating nucleons or participant constituents for production of different varieties of hadrons. The obtained values of q and T_0 show strong centrality dependences for both $Au+Au$ and $D+Au$ collisions. In all cases, the solid lines/curves represent model-based results and the data-points were obtained mostly by PHENIX and STAR at RHIC-BNL in USA. All the model-based fits are based here on Eq. (9). The different values of the fit parameters for production of various secondaries are listed in Tables 1 to 4. The performance of the present non-extensive approach *vis-a-vis* the studied ranges of experimental data is quite appreciable as can be seen from the χ^2/ndf-values given in the last column of each table.

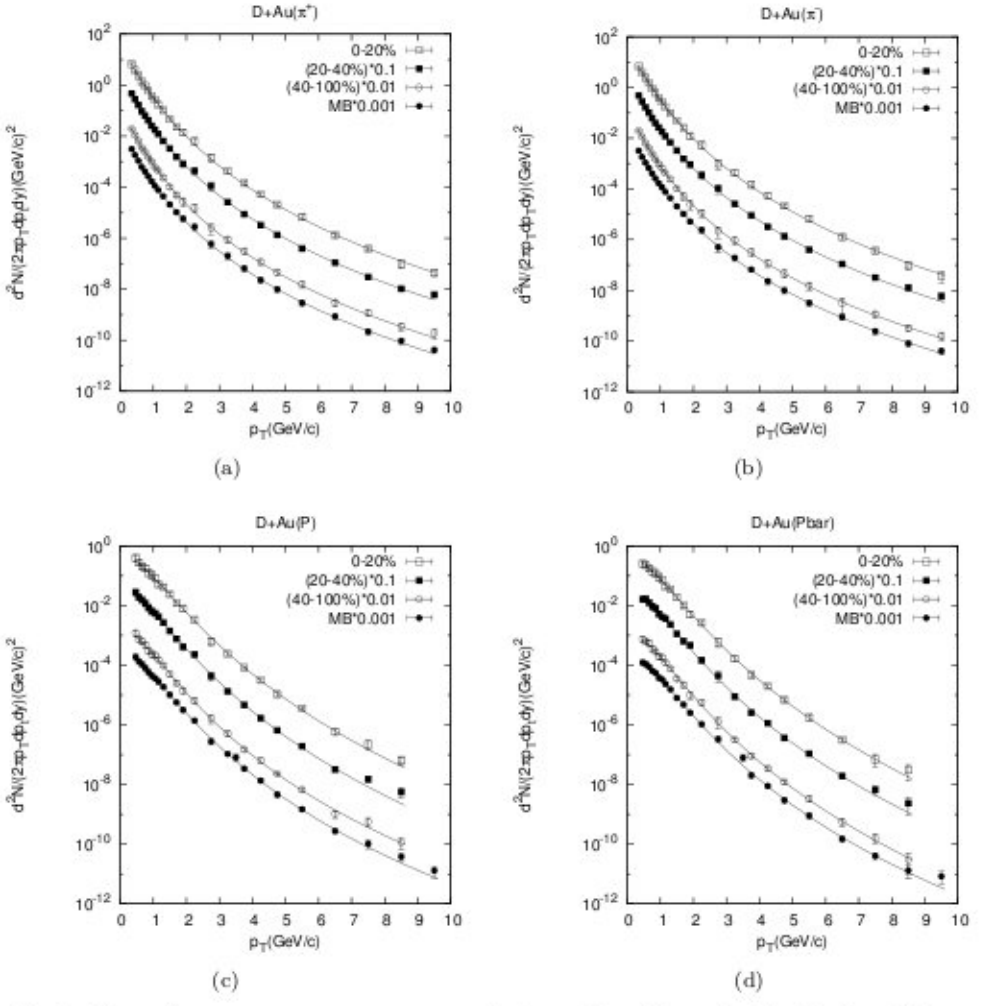

Fig. 3. Plots of transverse momentum spectra of π^+, π^-, P and $\bar{P}$ produced in $D+Au$ collisions at $\sqrt{s} = 200$ GeV at different centralities. The filled symbols represent the experimental data points.[10–12] The solid curves provide the fits on the basis of nonextensive approach (Eq. (9)).

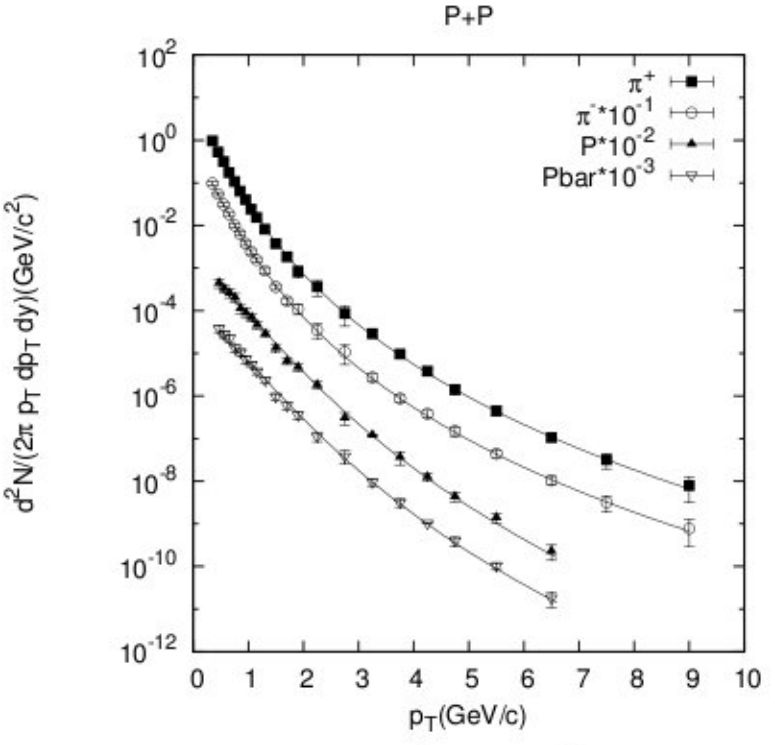

Fig. 4. Plots of transverse momentum spectra of π^+, π^-, P and $\bar{P}$ produced in $P+P$ collisions at $\sqrt{s} = 200$ GeV at different centralities. The filled symbols represent the experimental data points.[10–12] The solid curves provide the fits on the basis of nonextensive approach (Eq. (9)).

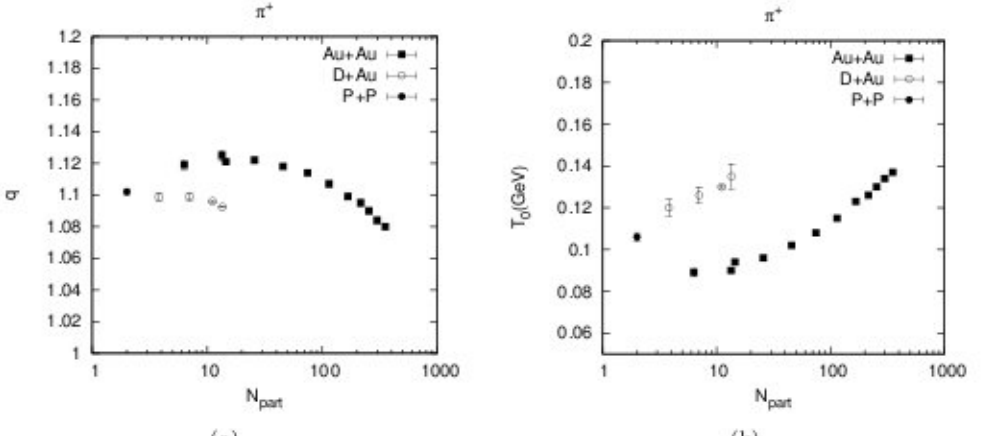

Fig. 5. Plots of (a) the nonextensive parameter q, and (b) the temperature T_0 as a function of number of participant nucleons in $Au + Au$, $D + Au$ and $P + P$ collisions at $\sqrt{s} = 200$ GeV.

Table 1. Values of fitted parameters with respect to experimental data on π^+-spectra at different centralities of $Au + Au$, $D + Au$ and $P + P$ collisions at RHIC.

	Centrality	C	q	T_0(GeV)	χ^2/ndf
$Au + Au$	0–5	7963 ± 198	1.080 ± 0.002	0.137 ± 0.001	35.180/25
	5–10	7000 ± 180	1.084 ± 0.002	0.134 ± 0.001	33.758/25
	10–15	6500 ± 170	1.090 ± 0.002	0.130 ± 0.001	28.543/25
	15–20	6010 ± 160	1.095 ± 0.002	0.126 ± 0.001	27.543/25
	20–30	4915 ± 123	1.099 ± 0.002	0.123 ± 0.001	28.704/25
	30–40	3873 ± 114	1.107 ± 0.002	0.115 ± 0.001	31.913/25
	40–50	2918 ± 53	1.114 ± 0.001	0.108 ± 0.001	21.123/25
	50–60	2089 ± 45	1.118 ± 0.001	0.102 ± 0.001	22.208/25
	60–70	1324 ± 40	1.122 ± 0.002	0.096 ± 0.001	24.902/25
	70–80	769 ± 32	1.125 ± 0.003	0.090 ± 0.001	19.718/25
	80–92	408 ± 23	1.119 ± 0.003	0.089 ± 0.002	14.443/25
	60–92	815 ± 24	1.121 ± 0.001	0.094 ± 0.001	12.717/25
	Min. Bias	3003 ± 36	1.091 ± 0.001	0.128 ± 0.001	24.140/25
$D + Au$	0–20	259 ± 51	1.092 ± 0.003	0.135 ± 0.006	5.682/21
	20–40	196 ± 4	1.096 ± 0.001	0.130 ± 0.001	7.505/21
	40–100	107 ± 13	1.099 ± 0.002	0.120 ± 0.004	5.022/21
	Min. Bias	145 ± 21	1.099 ± 0.002	0.126 ± 0.004	5.077/21
$P + P$	—	81 ± 6	1.102 ± 0.002	0.106 ± 0.002	2.813/20

Table 2. Values of fitted parameters with respect to experimental data on π^--spectra at different centralities of $Au + Au$, $D + Au$ and $P + P$ collisions at RHIC.

	Centrality	C	q	T_0(GeV)	χ^2/ndf
$Au + Au$	0–5	7032 ± 111	1.074 ± 0.001	0.143 ± 0.001	38.177/25
	5–10	6551 ± 98	1.081 ± 0.001	0.138 ± 0.001	34.642/25
	10–15	5805 ± 120	1.086 ± 0.001	0.134 ± 0.001	31.759/25
	15–20	5313 ± 91	1.091 ± 0.001	0.130 ± 0.001	29.390/25
	20–30	4325 ± 78	1.095 ± 0.001	0.127 ± 0.001	32.653/25
	30–40	3508 ± 87	1.105 ± 0.001	0.118 ± 0.001	32.142/25
	40–50	2628 ± 51	1.111 ± 0.001	0.111 ± 0.001	37.299/25
	50–60	1850 ± 38	1.116 ± 0.001	0.105 ± 0.001	28.672/25
	60–70	1137 ± 32	1.118 ± 0.002	0.099 ± 0.001	25.150/25
	70–80	693 ± 32	1.124 ± 0.002	0.092 ± 0.001	26.943/25
	80–92	389 ± 16	1.120 ± 0.003	0.089 ± 0.001	14.389/25
	60–92	718 ± 20	1.119 ± 0.001	0.097 ± 0.001	22.894/25
	Min. Bias	2576 ± 48	1.085 ± 0.001	0.134 ± 0.001	30.389/25
$D + Au$	0–20	280 ± 47	1.093 ± 0.003	0.132 ± 0.006	4.431/21
	20–40	206 ± 30	1.096 ± 0.008	0.129 ± 0.009	5.528/21
	40–100	117 ± 17	1.099 ± 0.003	0.118 ± 0.004	2.593/21
	Min. Bias	163 ± 11	1.101 ± 0.001	0.122 ± 0.002	2.526/21
$P + P$	—	90 ± 7	1.103 ± 0.002	0.103 ± 0.002	2.410/20

Table 3. Values of fitted parameters with respect to experimental data on P-spectra at different centralities of $Au+Au$, $D+Au$ and $P+P$ collisions at RHIC.

	Centrality	C	q	T_0(GeV)	χ^2/ndf
	0–5	204 ± 6	1.023 ± 0.002	0.288 ± 0.003	35.738/19
	5–10	173 ± 6	1.023 ± 0.002	0.287 ± 0.003	37.085/19
	10–15	148 ± 4	1.023 ± 0.001	0.286 ± 0.002	32.080/19
	15–20	123 ± 3	1.024 ± 0.001	0.285 ± 0.002	30.525/19
	20–30	104 ± 3	1.026 ± 0.001	0.278 ± 0.002	29.832/19
	30–40	105 ± 7	1.036 ± 0.002	0.251 ± 0.004	28.570/19
$Au+Au$	40–50	102 ± 9	1.046 ± 0.002	0.224 ± 0.005	27.118/19
	50–60	101 ± 2	1.053 ± 0.001	0.200 ± 0.001	24.202/19
	60–70	108 ± 9	1.063 ± 0.001	0.170 ± 0.003	26.689/19
	70–80	98 ± 5	1.069 ± 0.001	0.147 ± 0.001	24.383/19
	80–92	75 ± 2	1.061 ± 0.001	0.140 ± 0.001	37.141/19
	60–92	107 ± 2	1.070 ± 0.001	0.151 ± 0.001	24.174/19
	Min. Bias	117 ± 4	1.039 ± 0.001	0.247 ± 0.001	25.963/19
	0–20	248 ± 15	1.077 ± 0.001	0.148 ± 0.001	8.003/19
$D+Au$	20–40	199 ± 17	1.078 ± 0.002	0.144 ± 0.002	10.619/19
	40–100	145 ± 10	1.081 ± 0.001	0.128 ± 0.001	8.924/19
	Min. Bias	174 ± 9	1.081 ± 0.002	0.137 ± 0.002	10.904/21
$P+P$	—	73 ± 3	1.075 ± 0.001	0.124 ± 0.001	14.295/17

Table 4. Values of fitted parameters with respect to experimental data on $\bar{P}$-spectra at different centralities of $Au+Au$, $D+Au$ and $P+P$ collisions at RHIC.

	Centrality	C	q	T_0(GeV)	χ^2/ndf
	0–5	195 ± 12	1.029 ± 0.001	0.271 ± 0.002	36.201/19
	5–10	183 ± 13	1.032 ± 0.001	0.264 ± 0.003	32.281/19
	10–15	177 ± 14	1.037 ± 0.001	0.255 ± 0.003	31.309/19
	15–20	173 ± 14	1.040 ± 0.002	0.246 ± 0.003	33.994/19
	20–30	171 ± 17	1.043 ± 0.001	0.232 ± 0.003	32.377/19
	30–40	167 ± 6	1.048 ± 0.001	0.214 ± 0.001	30.771/19
$Au+Au$	40–50	151 ± 7	1.054 ± 0.001	0.197 ± 0.001	33.066/19
	50–60	139 ± 24	1.057 ± 0.002	0.180 ± 0.004	28.989/19
	60–70	120 ± 18	1.064 ± 0.003	0.160 ± 0.004	22.282/19
	70–80	98 ± 25	1.068 ± 0.002	0.141 ± 0.006	18.541/19
	80–92	90 ± 10	1.065 ± 0.001	0.131 ± 0.002	13.448/19
	60–92	110 ± 15	1.070 ± 0.001	0.145 ± 0.003	15.041/19
	Min. Bias	122 ± 14	1.045 ± 0.001	0.230 ± 0.004	34.014/19
	0–20	296 ± 19	1.074 ± 0.002	0.142 ± 0.002	5.202/19
$D+Au$	20–40	280 ± 15	1.075 ± 0.001	0.134 ± 0.002	8.770/19
	40–100	151 ± 9	1.076 ± 0.002	0.126 ± 0.002	5.812/19
	Min. Bias	216 ± 15	1.079 ± 0.009	0.131 ± 0.008	0.417/20
$P+P$	—	58 ± 1	1.076 ± 0.003	0.124 ± 0.003	19.067/17

4. On the Physics of q-Statistics

4.1. *Heavy ion collisions and the interpretation for evolution of q-statistics in them*

Let us start with a few ansatz to be made on the nature of heavy ion collisions which are modestly well-indicated by the recent experiments: (i) Heavy ion collisions involve collisions of a large number of the constituent nucleons and their partons at high energies. (ii) Obviously, such multiple collisions over a certain length of time make the process a long-ranged one, i.e., the process of equilibration takes a much longer time than the time to traverse the mean free path of collisions. (iii) So,

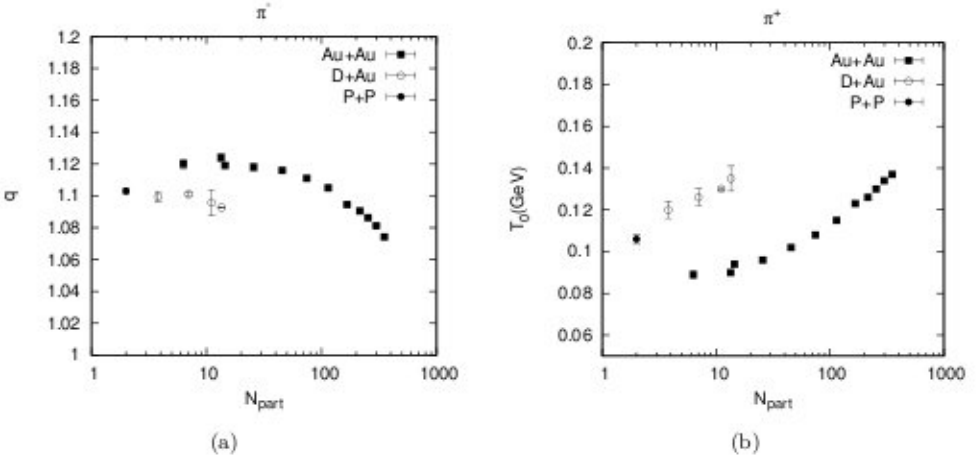

Fig. 6. Plots of the nonextensive parameter q and the temperature T_0 as a function of number of participant nucleons in $Au + Au$, $D + Au$ and $P + P$ collisions at $\sqrt{s} = 200$ GeV.

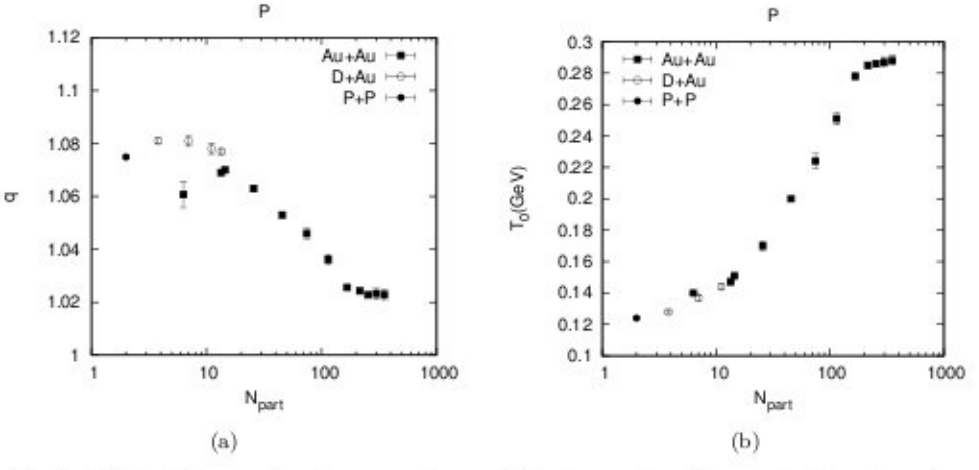

Fig. 7. Plots of the nonextensive parameter q and the temperature T_0 as a function of number of participant nucleons in $Au + Au$, $D + Au$ and $P + P$ collisions at $\sqrt{s} = 200$ GeV.

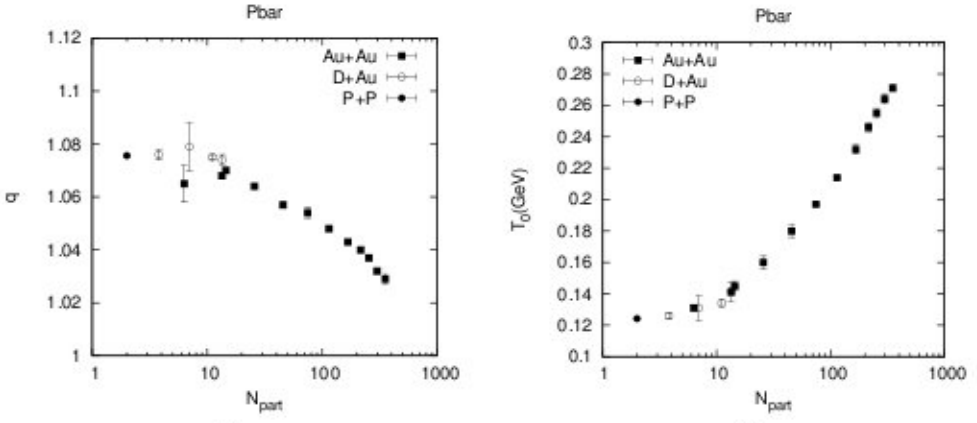

Fig. 8. Plots of the nonextensive parameter q and the temperature T_0 as a function of number of participant nucleons in $Au + Au$, $D + Au$ and $P + P$ collisions at $\sqrt{s} = 200$ GeV.

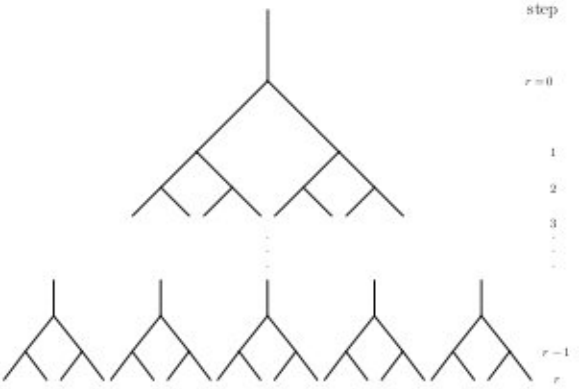

Fig. 9. The self-similar cascade with fractal properties.

from the very onset of the interaction taking place, the system has the tendency of transitions to chaos. (iv) Such transitions from somewhat periodic to chaotic behavior is mediated by, as in other cases of complexity phenomena, the appearance of a multifractal "critical" attractor with moderately well-known geometrical properties. Such critical attractors have a vanishing Lyapunov coefficient and a sensitivity to initial conditions, say ξ_t, that do not converge to any single-valued function but instead display a fluctuating pattern that grows as a power law in time. Besides, trajectory within such a critical attractor show self-similar temporal cascadised structures as is evinced by the following particle-production[13] diagram (Fig. 9). The added property is: they preserve memory of their previous locations and do not have the mixing property of truly chaotic trajectories. Such a scenario is also marked by the occurrence of a so-called q-phase dynamical phase transition.

And one knows very well that heavy ion collisions are, *ab initio*, a study into the suspect state of phase-transitions.

4.2. *q-Statistics for the critical attractors*

Manifestation of the q-statistics in the dynamics at a critical attractor is conditioned by two criteria. The first property is its (finite time) sensitivity to initial condition, ξ_t, and defined by

$$\xi_t(x_{\text{in}}) = \exp_q(\lambda_q(x_{\text{in}})t) \tag{10}$$

where Δx_{in} is the initial separation of two trajectories and Δx_t is the same at time t, q is the entropic index, $\lambda_q(x_{\text{in}})$ is the q-generalized Lyapunov coefficient and $\exp_q(x) = [1-(q-1)x]^{\frac{-1}{q-1}}$ is the q-exponential function. The second property pertains to temporal extensively of entropy production at critical attractors. That is, linear growth with time of the entropy associated to an ensemble of trajectories. The expression for the rate of entropy-production $K_q(x_{\text{in}})$ is taken to be given by

$$K_q(x_{\text{in}})t = S_q(t, x_{\text{in}}) - S_q(0, x_{\text{in}}) \tag{11}$$

where

$$S_q = \Sigma p_i \ln_q p_i^{-1} = \frac{1 - \Sigma_q^W p_i^q}{q-1} \tag{12}$$

is the Tsallis entropy and where $p_i(t)$ is the distribution of the trajectories in the ensemble at time t given that they were distributed initially within a small interval around x_{in}.

Two points are to be noted here. Firstly, one notes that $\ln_q(y) \equiv (y^{1-q} - 1)/(1-q)$ is the inverse of $\exp_q(y)$. Secondly, all quantities in the aforementioned expressions are quite clearly dependent on the initial position x_{in}.

Some other comments are also in order:

(i) Because of the memory retention of the trajectories the dependence on x_{in} in Eq. (10) (or Eq. (11)) does not disappear for sufficiently large t. The notable feature here is the usual large t limiting condition not present in the definition of ξ_t in Eq. (10) or in Eq. (11).

(ii) Besides, it is anticipated that the index q in Eq. (9) takes a well-defined value determined by the basic attractor properties such as its universal constants. For a multifractal critical attractor there may be a distinct discrete family of such values for q.

In fact, the elements of q-statistics give rise to many other important associated characteristics[14] of the critical attractors which play crucial role in the heavy ion collision.

5. Discussion and Conclusions

The plots in various figures (Figs. 1 to 4) not only provide good fits to the experimental data, but also reveal the strength of non-extensive approach in parallel to the existing exponential- and power-law-based models. The exponential laws take care of mainly the soft-p_T region of the hadronic spectra while the QCD-inspired power-law models perform well in the hard-p_T region, i.e., the region of high transverse momentum. But the present approach, as evidenced from the graphs and χ^2/ndf-values, does not distinguish between such low and high-p_T regions, rather it provides quite good fits to the data over the whole p_T region in a unified manner. So this provides a technical tool to present soft and hard physics in an integrated manner.

The graphs represented by Figs. 5(a) to 5(b) and Figs. 7(a) to 7(b) reveal some striking features at first glance. The number of participant nucleons, N_{part}, for central to peripheral $D + Au$ collisions match with the same for $Au + Au$ collisions mainly in the peripheral regions. But the obtained values of q and T_0 for $D + Au$ and $Au + Au$ collisions do not match at all in the specified region of N_{part}. Actually, for nearly same values of N_{part}, as seen from the Figs. 5(a) to 5(b), the non-extensivity is quite high and the Hagedorn temperature is relatively low in $Au + Au$ collision compared to $D + Au$ interactions. On the other hand, the values of q and T_0 obtained for $P + P$ collision, along with $D + Au$, exhibits a systematic trend. It may seem surprising. But the reason lies in the fact that for $Au + Au$ collisions the data exist only for the values $p_T < 3.0$ GeV/c; while a wider range of data ($0.35 \leq p_T \leq 9.5$ GeV/c) have been taken into account for some other collisions here. The particles with $p_T < 3.0$ GeV/c are generally emitted at much lower temperature than those with higher transverse momentum ($p_T > 5$ GeV/c). Hence, obtaining a lower temperature value for pion-spectra in $Au + Au$ collisions is not very surprising.

The non-extensivity parameter, q is related directly with the fluctuations in temperature.[8] The high value of q reflects high fluctuations in temperature, T_0. And a system with a higher fluctuation in temperature means the system is far away from its thermal equilibrium. The high q-values obtained from the π^+-spectra of $Au + Au$ collisions compared to $D + Au$ and $P + P$ collisions indicate that those positive pions from $Au + Au$ collision with momenta lying in the low and intermediate regions were evolved from a region of the fireball which had yet to reach its thermal equilibrium.

Quite spectacularly, the trends of the plots of Fig. 5(a) and Fig. 5(b) and of the rest are in contrast. But this is only apparent. Essentially, they represent fully the physical consistency of the non-extensive picture. The number of collisions is maximum for the most central collisions for which the temperature would try to gradually ascend with increasing N_{part}. The physical scenario then speedily proceeds towards equilibrium which signals the observed diminishing trend of the non-extensivity parameter, q in Fig. 5(a) and the (a)-marked figures in all of the rest.

References

1. C. Tsallis, *J. Stat. Phys.* **52** (1988) 479; *Physica A* **221** (1995) 277; *Braz. J. Phys.* **29** (1999) 1; D. Prato and C. Tsallis, *Phys. Rev. E* **60** (1999) 2398.
2. C. Beck, *Physica A* **286** (2000) 164.
3. C. Beck, *Physica A* **305** (2002) 209.
4. G. Wilk and Z. Wlodarczyk, *Chaos, Solitons and Fractals* **13** (2002) 581.
5. G. Wilk and Z. Wlodarczyk, *Physica A* **305** (2002) 227.
6. T. S. Biro *et al.*, hep-ph/0409157.
7. T. S. Biro and G. Purcsel, *Phys. Rev. Lett.* **95** (2005) 162302.
8. M. Biyajima *et al.*, hep-ph/0403063.
9. M. Biyajima *et al.*, hep-ph/0602120.
10. PHENIX Collaboration (S. S. Adler *et al.*) *Phys. Rev. C* **69** (2004) 034909.
11. STAR Collaboration (J. Adams *et al.*) *Phys. Lett. B* **616** (2005) 8.
12. STAR Collaboration (J. Adams *et al.*) nucl-ex/0601033.
13. I. Sarcevic, *Proceedings of Large Hadron Collider Workshop*, Vol. II, eds. G. Jarlskog and D. Rein (CERN 90–10 & ECFA 90–133, 3 December 1990), p. 1218.
14. A. Robledo, cond-mat/0606334 v1 (June 2006).